July 2004

Surface composition and structure of $Co_3O_4(110)$ and the effect of impurity segregation

S.C. Petitto
University of Nebraska - Lincoln

Marjorie Langell
University of Nebraska - Lincoln, mlangell1@unl.edu

Surface composition and structure of $Co_3O_4(110)$ and the effect of impurity segregation

S. C. Petitto and M. A. Langell[a)]
Department of Chemistry, University of Nebraska, Lincoln, Nebraska 68588-0304

(Received 8 October 2003; accepted 26 April 2004; published 22 July 2004)

The $Co_3O_4(110)$ single crystal surface has been characterized by low energy electron diffraction (LEED), Auger electron spectroscopy, and x-ray photoelectron spectroscopy (XPS). LEED analysis of the clean $Co_3O_4(110)$ spinel surface shows a well-ordered pattern with sharp diffraction features. The XPS spectra are consistent with stoichiometric Co_3O_4 as determined by the concentration ratio of oxygen to cobalt (C_O/C_{Co}) and spectral peak shape. In particular, the cobalt $2p$ XPS spectra are characteristic of the spinel structure with Co^{3+} occupying octahedral sites and Co^{2+} in tetrahedral sites within the lattice. During prolonged heating at 630 K, bulk impurities of K, Ca, Na, and Cu segregated to the surface. Sodium desorbed from the surface as NaOH at 825 K, potassium and calcium were only removed by sputtering since no desorption from the surface was detected for temperatures up to 1000 K. Copper also disappeared upon heating above 700 K, most likely by desorbing although the possibility of diffusion back into the bulk could not be eliminated. The appearance of copper impurities correlated with $Co_3O_4(110)$ surface reduction to CoO, and the surface could not be fully reoxidized even upon extended oxygen annealing as long as the copper impurity remained on the surface. Upon removal of the Cu from the near-surface region, the surface was easily reoxidized to Co_3O_4 by O_2. © *2004 American Vacuum Society.*
[DOI: 10.1116/1.1763899]

I. INTRODUCTION

Transition metal oxides play an important role in a variety of technological applications and heterogeneous processes. Industrially, a cobalt oxide spinel, Co_3O_4, is used at room temperature for ethene hydrogenation[1] and oxidation of carbon monoxide.[1–4] Co_3O_4 is also used in low temperature catalytic converters in fuel-efficient engines,[5] as solid state gas sensors for carbon monoxide and hydrogen gas monitoring,[6] and as a coating in fuel cells.[7] One characteristic that makes Co_3O_4 ideal for usage in these extreme environments is its excellent anticorrosion properties.[4] In-depth understanding of metal–oxide surface structure and reactivity is crucial to continued development of the technological performance and efficiency of Co_3O_4-based materials applications.

Cobalt-containing mixed-metal oxide spinels have also been studied for their ability to tailor the chemical and physical properties of a substrate. As with Co_3O_4, $Cu_xCo_{3-x}O_4$ has high catalytic activity towards CO oxidation in engine exhausts. The $Cu_xCo_{3-x}O_4$ catalysis is less susceptible to catalytic poisoning by SO_2 than Co_3O_4;[8,9] therefore, adding copper to the Co_3O_4 spinel structure increases the lifetime and productivity of the catalyst. Other transition metals have been used to alter Co_3O_4 properties as well. For example, oxygen electrodes and cathodic materials have been fabricated with $Mn_xCo_{3-x}O_4$ for its electrocatalyic properties,[10] and $NiCo_2O_4$ has interesting magnetic and ferromagnetic properties, along with electrochemical properties for oxygen evolution electrodes.[11]

Co_3O_4 has a cubic spinel structure with a lattice constant of 8.084 Å (Ref. 12) and 56 atoms in the unit cell. Thirty-two O^{2-} anions are packed in the face-centered-cubic (fcc) lattice structure with 16 of the octahedral sites occupied by Co^{3+} cations and 8 of the tetrahedral sites occupied by Co^{2+} cations.[13] Co_3O_4 single crystals generally form in a truncated octahedron morphology with naturally occurring (110) and (111) crystal faces.[13,14] The CoO rocksalt structure is easily related to that of the Co_3O_4 spinel. The CoO lattice is also fcc in O^{2-}, but has all its octahedral cations sites occupied by Co^{2+} and no occupied tetrahedral sites. The most stable rocksalt surface is CoO(100). CoO is a charge-transfer insulator with a band gap of 6 eV,[15] while Co_3O_4, which tends to be a p-type semiconductor by nature, has a band gap of about 2.2 eV.[16]

The surface chemical composition of the stoichiometric spinel has been previously studied using x-ray photoelectron spectroscopy (XPS). Characteristic of the Co_3O_4 spinel surface is a set of sharp Co $2p$ peaks at 779.8 and 795.7 eV with a broad satellite structure located about 9 eV higher in binding energy[10,15,17–23] than the main peaks. The satellite structure is very weak in intensity in comparison to that of CoO,[15] whose very intense satellite features are commonly used to identify cobalt-containing oxides as the rocksalt monoxide. The cobalt $2p$ spectrum obtained for the stoichiometric $Co_3O_4(110)$ crystal is consistent with Co^{3+} cations occupying octahedral sites and Co^{2+} cations in tetrahedral sites within the fcc O^{2-} sublattice.[15,17–19,24–26]

We present here a study of stoichiometric $Co_3O_4(110)$ and Cu impurity segregated $Co_3O_4(110)$ surfaces. The (110) surface structure and chemical compositions were investigated using Auger electron spectroscopy (AES), XPS, and low energy electron diffraction (LEED). Some alkali, cal-

a)Corresponding author; electronic mail: mlangell@unlserve.unl.edu

cium, and copper impurities were observed to segregate from the bulk upon prolonged heating, and the presence of copper, in particular, affected the chemical composition of the surface. The Co_3O_4(110)−Cu surface is reduced to a CoO-like composition and cannot be fully reoxidized as long as copper remains on the surface. The Co_3O_4 LEED pattern is representative of a cubic (110) surface[27] with increasing complexity at higher incident energies as fractional-ordered spots come into and out of focus. The Cu-segregated, reduced surface LEED pattern shows a different surface structure than that of the clean, stoichiometric Co_3O_4(110) surface.

II. EXPERIMENT

The Co_3O_4 single crystal sample was grown from a molybdenum electrolytic flux with naturally occurring (110) and (111) faces.[28] A single crystal with an approximately 3 mm $\times$3 mm (110) sample face was held in place using a wrap constructed out of 0.025 mm thick gold foil (Alfa Aesar, 99.95%), with care taken not to obscure the crystal face. Two tantalum wires, (0.25 mm diameter, Alfa Aesar, 99.9±%), were wound around the wrapped sample, and the sample was suspended between two heating posts by the heating wires. The manipulator had provisions for resistive heating through the Ta wires and cooling with a liquid-nitrogen cryostat over a temperature range of 100–1000 K. The temperature was measured with a Chromel–Alumel thermocouple spot welded to the gold foil at the back of the sample.

XPS spectra of several compounds with well-defined surfaces are given as reference in Co $2p$ photoemission characterization. Preparation and characterization of these surfaces have been reported previously. Briefly, the CoO single crystal was obtained from Atomeric Chemetals Corp. and was grown by the flame fusion method. The crystal surface was cleaved, polished, and oriented along the (100) plane to within 0.5° using back Laue diffraction and characterized by a number of surface-sensitive techniques.[17–19] Thin films of Co_3O_4 were grown on the CoO(100) single crystal by annealing under O_2 (6×10^{-5} Pa) at 625 K for several hours. Details of this procedure and subsequent characterization of the surface quality can be found in Refs. 17–19. Nickel cobalite ($NiCo_2O_4$), was prepared by standard sol–gel methods, described in Ref. 11, along with characterization of its surface by AES and XPS.

After the Co_3O_4 single crystal was introduced into ultrahigh vacuum (UHV) (base pressure $\sim3\times10^{-8}$ Pa), the sample was cleaned using repeated cycles of Ar^+ sputtering (4×10^{-3} Pa Ar^+, 2.3 μA/cm^2) for 30 min at 300 K, followed by annealing under O_2 (1.3×10^{-5} Pa) for 20 min at 630 K, and annealing under UHV for 10 min at 630 K. The UHV anneal removes any excess surface oxygen from the previous O_2 anneal. The cleanliness and stoichiometry of the sample were determined by AES. AES spectra were obtained using a Physical Electronics (Φ) 15–255 G double-pass cylindrical mirror analyzer (DPCMA) with a 2 kV primary electron beam. The sample was considered clean when contaminants were below the level of AES detection.

The Co_3O_4(110) LEED patterns were obtained using Vacuum Generator 8011 rear view four grid LEED optics with primary beam energies of 30–150 eV. The diffraction patterns were recorded and analyzed using EE2000 SMARTOOL software.

XPS data were taken using both Mg and Al $K\alpha$ photon sources ($h\nu=1253.6$ and 1486.6 eV, respectively) using a Φ 04-548 dual anode x-ray source controlled by a Φ 50-096 x-ray source control/supply. The Φ 15-255G DPCMA was also used to obtain XPS data with a 25 eV pass energy. The binding energies were calibrated to the Co_3O_4 lattice O $1s$ peak at 529.6 eV to compensate for any charging effects. All XPS data were analyzed after the removal of a Shirley background[29] and fitted with a minimum number of Gaussian–Lorentzian peaks using XPSPEAK 4.1.[30]

III. RESULTS

The as-introduced AES spectrum indicates several surface contaminants, the most common being potassium, carbon, and calcium. These contaminants are estimated to be in submonoloayer coverage based on their Auger intensities and can be removed by Ar^+ sputtering. Compositional information is also obtained from XPS data. The relative surface concentration of oxygen to cobalt can be estimated using integrated XPS intensity values (I_i) and the appropriate sensitivity factors (S_i) with $S_{Co}/S_O=5.43$.[31,32] The calculated concentration ratio of oxygen to cobalt (C_O/C_{Co}),

$$\frac{C_O}{C_{Co}}=\frac{I_O/S_O}{I_{Co}/S_{Co}}, \tag{1}$$

is 1.28±0.15, also in agreement with the stoichiometric ratio[17,33] to within error.

A comparison of cobalt $2p$ regions for several cobalt oxides is shown in Fig. 1. Co_3O_4 in its various forms of preparation and Co^{3+}-containing $NiCo_2O_4$ have binding energies at 779.8 and 795.7 eV for $2p_{3/2}$ and $2p_{1/2}$, respectively.[3,8–11,16–20,22–24,26] CoO $2p$ binding energies are higher, 780.5 and 796.6 eV.[3,11,15,17–21] Weak $2p$ satellite features for the spinels are found at 788.8 and 804.2 eV,[3,8–11,17–20,22–24,26] with significantly reduced intensity compared to the intense CoO satellites, which are found at lower binding energies of 785.5 and 802.1 eV.[11,17–20] The weak satellite structures of Co_3O_4 and $NiCo_2O_4$ are characteristic of spinel structures in which 3^+ cations occupy octahedral lattice sites with diamagnetic, filled t_{2g} and empty e_g levels, and 2^+ cations are in tetrahedral sites.[15,17–19,24–26] CoO 2^+ cations are high spin d^8 in octahedral lattice sites and the intense satellite structure has been proposed to result from the charge-transfer band structure found in late $3d$ transition metal monoxides with partially filled e_g character.[15,16,25,33–35]

The unpaired nature of the half-filled e_g band of the Co^{2+} cation in CoO results in strong electron correlation and substantial broadening of the cobalt $2p$ main peaks due to many closely lying $3d$ final states in photoemission. In contrast, the low-spin, diamagnetic nature of the Co^{3+} octahedral cation and the weaker crystal field effect of tetrahedral coordination for the Co^{2+} cation result in similar photoemission

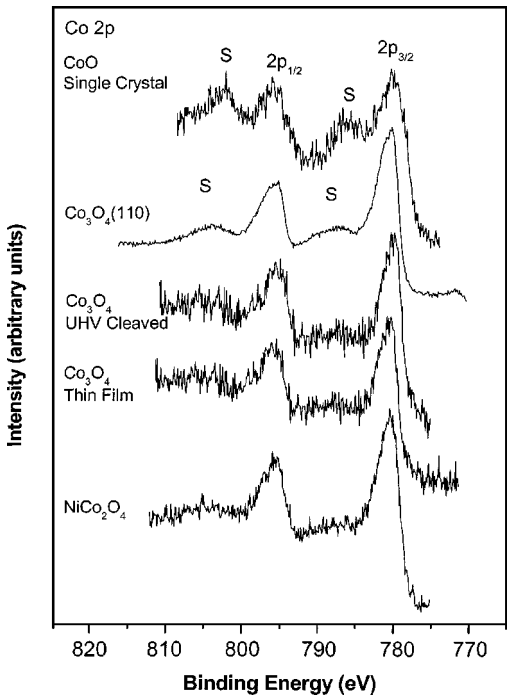

FIG. 1. Comparison of Co $2p$ XPS spectra of cobalt oxides with varying cobalt chemical environments: CoO single crystal (Ref. 17), Co_3O_4 single crystal cleaved in UHV (Ref. 11), Co_3O_4 thin film (Ref. 17), and $NiCo_2O_4$ (Ref. 11). Only Co^{2+} in octahedral sites shows a significant satellite structure.

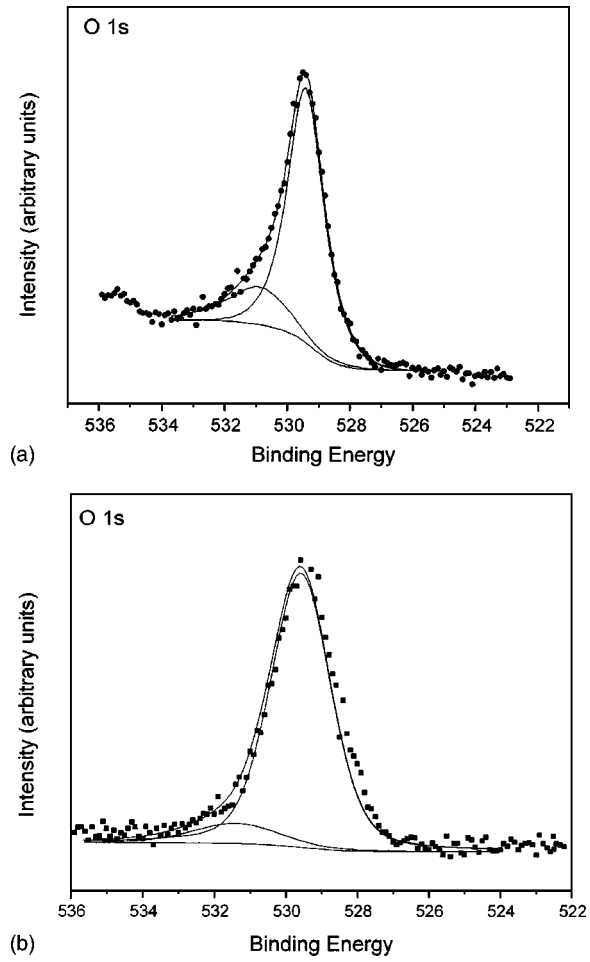

FIG. 2. Oxygen $1s$ XPS spectra of (a) $Co_3O_4(110)$ and (b) $Co_3O_4(110)-Cu$ fitted with a Shirley background and two Lorentzian–Gaussain peaks acquired with Mg $K\alpha$ radiation.

binding energies and a sharper $2p$ peak for the spinel, despite the existence of two different cobalt oxidation states in this material. Thus the satellite structures, not absolute $2p_{3/2}/2p_{1/2}$ binding energies, are better able to distinguish between rocksalt CoO and cobalt-containing spinels with octahedrally coordinated Co^{3+}.

The O $1s$ region for the clean, stoichiometric $Co_3O_4(110)$ single crystal is shown in Fig. 2(a). The main oxygen peak due to lattice O^{2-} is set to 529.6 eV, as has been previously found for CoO,[13,17–21,36] Co_3O_4,[3,10,17–19,22,23,34] and the spinels; $Cu_xCo_{3-x}O_4$,[8] $Mn_xCo_{3-x}O_4$,[10] and $NiCo_2O_4$.[11,37] There is a second peak at higher binding energy, 531.1 eV at 10%–15% intensity of the main peak. The 531.1 eV binding energy is comparable to that reported for surface hydroxyls,[3,8,10,26,38–40] under-coordinated lattice oxygens (O^-),[20,21,36] chemisorbed oxygen,[41] and inaccuracies in the peak fitting due to the inability to reproduce the exact peak shape and/or secondary electron background. O $1s$ peaks with comparable binding energy have also been observed on Co_3O_4 thin films,[17–19,22,35] on Co_3O_4 powder surfaces,[23,42] and in a Co_3O_4 single crystal cleaved in UHV.[11] While it is not possible to rule out defects or low levels of hydroxylation, the O $1s$ peak at 531.1 eV is probably at least partially attributable to the intrinsic O $1s$ peak structure, which is imperfectly reproduced in the peak fitting procedure. One indication of this in the present set of spectra is the broadness of the peak [full width at half maximum (FWHM) $=2.0$ eV] compared to the lattice peak (FWHM$=1.2$ eV). The very weak feature observed at 535.5 eV in Fig. 2(a) can be attributed to the lower binding energy shoulder of the Co Auger ($L_2M_{23}V$) transition.[39]

LEED patterns for $Co_3O_4(110)$ were obtained with incident energies of 36–147 eV (Fig. 3) and yield a well-ordered rectangular lattice representative of a cubic (110) spinel surface.[27] No sample charging was experienced over this energy range. The crystal structure of Co_3O_4 is a nonprimitive unit cell with 56 atoms with a complicated diffraction pattern in which multiple sets of diffraction features come into and out of focus as the primary beam energy is varied. There are two possible unreconstructed surface terminations for the (110) surface, type A and type B (Fig. 3). The clean $Co_3O_4(110)$ LEED diffraction patterns are representative of type A surface termination.[43]

After repeated cleaning cycles of annealing at 630 K under UHV, bulk impurities of K, Ca, Na, and Cu segregated to the surface [Fig. 4(b)]. The Auger peak intensities indicate the impurities to be present in submonolayer coverage with a maximum concentration of 1 K atom and 3 Ca atoms per 10 Co atoms if all the impurity atoms were present as an overlayer on top of a Co_3O_4 selvedge. There are no detectable Na peaks in the Auger spectrum because sodium is extremely susceptible to electron stimulation desorption under the con-

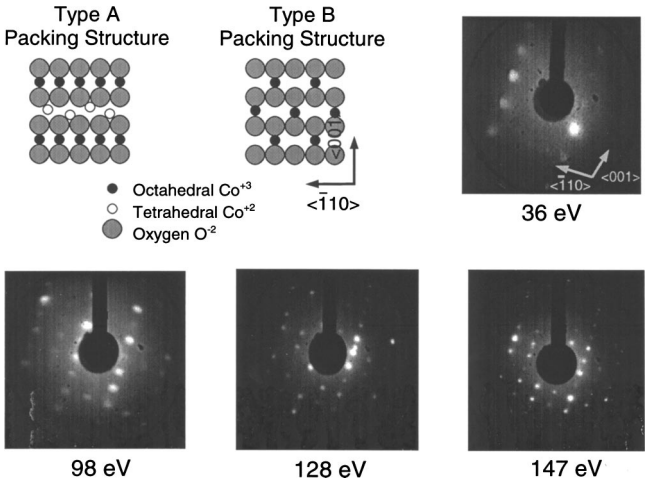

FIG. 3. Schematics of type A and type B (110) spinel surface termination (Ref. 43). LEED diffraction patterns of stoichiometric $Co_3O_4(110)$ at incident electron beam energies, 36–147 eV. The sharp diffraction features are representative of a (110) surface with a type A packing structure.

ditions used in Auger analysis. However, a weak sodium 1*s* photoemission peak was seen in the XPS at 1072.4 eV, representative of Na_2O,[32] and sodium was found to desorb from the surface as NaOH over a broad temperature range with a maximum at 850 K when heated at 15 K/s. The hydrogen in the desorbing NaOH presumably originates from background H_2 or H_2O. In attempts to increase Na desorption, the surface was treated with H_2O which had no effect on the amount or rate of sodium desorption, and the 531.1 eV O 1*s*

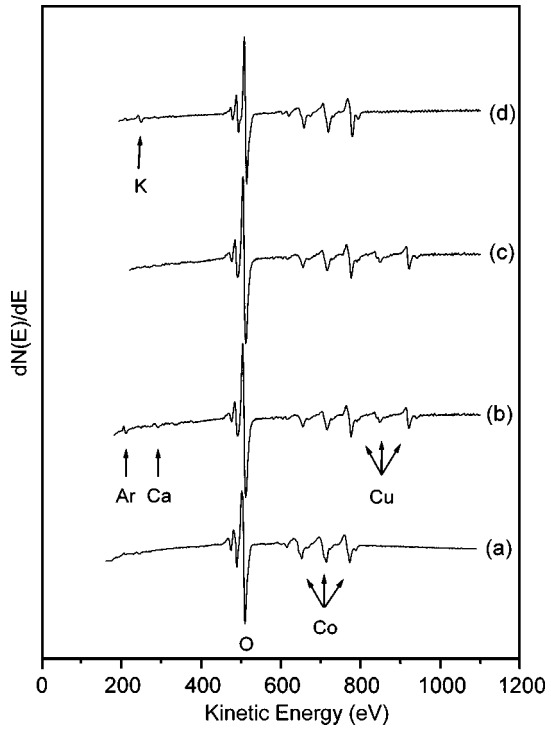

FIG. 4. AES spectra of (a) stoichiometric $Co_3O_4(110)$ (b) "dirty" $Co_3O_4(110)$–Cu, (c) "clean" $Co_3O_4(110)$–Cu, and (d) $Co_3O_4(110)$–Cu after heating from 300 to 900 K.

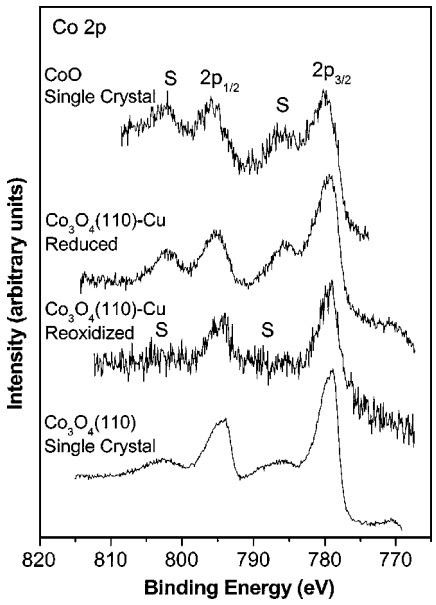

FIG. 5. Comparison of Co 2*p* XPS spectra of cobalt oxides with Co^{3+} and Co^{2+} chemical environments: CoO single crystal (Ref. 17), $Co_3O_4(110)$–Cu reduced surface, $Co_3O_4(110)$–Cu reduced surface reoxidized, and $Co_3O_4(110)$ single crystal.

peak intensity did not increase in intensity. Note that the alkali and calcium impurities were present to varying extents during copper segregation experiments. It was possible to obtain alkali and calcium impurities when copper was not present and it was also possible to detect copper with little or no alkali and calcium. The changes described below were only detected when copper was present and did not correlate with alkali or calcium impurity segregation.

The cobalt 2*p* XPS spectrum of the $Co_3O_4(110)$–Cu surface changes substantially as the surface is reduced. Peak shapes and intensity indicated a CoO-like surface with a intense satellite structure in the 2*p* spectrum (Fig. 5). From XPS, the calculated oxygen to cobalt concentration ratio for this copper segregated surface was found to be $C_O/C_{Co} = 0.94 \pm 0.15$. The Co 2*p* peaks were observed at 779.2 and 795.2 eV, within error of the binding energies reported for the spinel Co_3O_4 surface. The $2p_{3/2}$ peak of the reduced surface broadens toward the higher binding energy side, characteristic of metal monoxide CoO, a highly electron correlated system with three unpaired 3*d* electrons. Simultaneously, the Co 2*p* satellites shift toward lower binding energies, by about 3 eV, to 785.5 and 802.1 eV. The photoemission spectra of the O 1*s* region of the $Co_3O_4(110)$–Cu surface also show a small second peak at 531.1 eV with the same peak intensity relative to the lattice peak [Fig. 2(b)] as is found for the clean $Co_3O_4(110)$.[11,17–19,44] Table I summarizes the photoemission peak binding energies.

LEED patterns for the reduced $Co_3O_4(110)$–Cu surface were obtained over an incident energy range of 60–150 eV and a representative pattern at 128 eV is shown in Fig. 6. The copper segregated pattern is hexagonal and is not easily related to the underlying rectangular type A clean surface

TABLE I. XPS binding energies (in eV) of stoichiometric Co_3O_4(110), Co_3O_4(110)–Cu, CoO(100) single crystal, and Co_3O_4 thin film grown on CoO(100) single crystal.

Sample	Co $2p_{3/2}$ (eV)	Co $2p_{3/2}$ satellite (eV)	Co $2p_{1/2}$ (eV)	Co $2p_{1/2}$ satellite (eV)	O 1*s* (eV)
Co_3O_4(100)	779.8	788.8	795.7	804.2	529.6, 531.1
Co_3O_4(110)–Cu	779.2	785.5	795.2	802.1	529.6, 531.1
CoO(100)[a]	780.5	787.1	796.4	803.0	529.4
Co_3O_4 thin film on CoO(100)[b]	779.6, 780.5	787.9	796.2	803.8	529.4, 531.2

[a]XPS values are set to O 1*s* binding energy of 529.4 eV (after Ref. 20).
[b]Reference 17.

Co_3O_4(110) LEED pattern. The copper segregated pattern also shows some indication of charging effects and is not as well developed as that of the clean Co_3O_4 substrate, indicating a less well ordered overlayer. This diffraction pattern was only observed when copper was detected on the surface, and was not present on clean or sodium, potassium, and/or calcium contaminated Co_3O_4(110) surfaces. For Co_3O_4(110) with Na, Ca, and K impurities segregated onto the surface, but no Cu, the LEED pattern resembles that of the stoichiometric spinel Co_3O_4(110) surface of type A surface termination. The surface may indicate stabilization of the type B spinel surface termination, or may result from copper oxide or a mix of copper–cobalt oxide composition. Extensive LEED analysis of this structure is underway and will be reported elsewhere.

The segregated copper can be removed by heating the sample to $\geqslant$700 K. An AES spectrum after heating the Co_3O_4(110)–Cu surface to 900 K is shown in Fig. 4(d) and for this surface the copper peaks are below the limit of detection. It is now possible to totally reoxidize the substrate to Co_3O_4(110) as the XPS (Fig. 5), LEED, and AES are again in agreement with the clean stoichiometric spinel Co_3O_4. Although alkali and calcium were often detected on copper segregated Co_3O_4(110) it was possible to obtain Cu-segregated Co_3O_4 that showed no detectable impurities beyond that of Cu [Fig. 4(c)]. For this "clean" Co_3O_4(110)–Cu surface, the copper saturated at a concentration of 7 Cu atoms to 10 Co atoms if it is assumed that the copper atoms are homogeneously distributed in the selvedge.

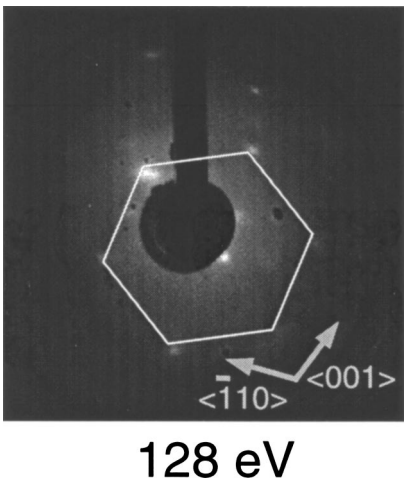

FIG. 6. Diffraction pattern of the Co_3O_4(110)–Cu overlayer at 128 eV incident energy. A new, although poorly developed, hexagonal structure has appeared and much of the Co_3O_4(110) pattern is obscured.

IV. DISCUSSION

Clean and impurity segregated Co_3O_4(110) surfaces were studied using AES, XPS, and LEED, where the clean Co_3O_4(110) data are consistent with the spinel structure and composition, and the Co_3O_4(110)–Cu data correspond to a CoO-like environment. The O 1*s* XPS spectra of both surfaces have been fitted with two oxygen peaks: lattice oxygen, set at a binding energy of 529.6 eV for calibration purposes, and a second higher binding energy peak at 531.1 eV. The latter, which is never more than 10%–15% of the lattice peak intensity, is believed to be largely intrinsic to the O 1*s* Co_3O_4 peak shape, a steady state low concentration of oxygen defects[34] or a terminal oxygen layer,[45] although the possibility of very low concentrations of surface hydroxyls is difficult to completely eliminate for any air exposed oxide sample. However, the extensive sputtering and extended high temperature anneals for the Co_3O_4(110) single crystal substrate make detectible levels of surface hydroxyls unlikely. A similar structure attributed to defects and/or adsorbed oxygen has been observed in Co_3O_4 thin films that did not show hydroxylation by high resolution electron energy loss spectroscopy (HREELS),[17–19] Co_3O_4 powder surfaces that were thermally treated to remove hydroxyls,[23] and UHV-cleaved Co_3O_4 single crystal surfaces.[31] Not only did the intensity of the peak not diminish after prolonged sputtering and high temperature anneals to 1000 K, but attempts to observe water or other hydroxylated desorption products with a quadrupole mass spectrometer by thermal desorption methods detected no such desorbing species.

Upon annealing to 630 K through repeated cleaning cycles under UHV, copper segregates to the Co_3O_4 surface over the course of several hours and saturates at 0.7 Cu atoms per Co substrate cation after approximately 20 h. The appearance of the copper impurity on the Co_3O_4(110) surface coincides with reduction of the cobalt oxide substrate and the formation of a CoO-like selvedge. The Co 2*p* XPS data show a satellite structure that is characteristic of a CoO-like environment, and the oxygen to cobalt atomic concentration decreases from 1.28 to 0.94 ± 0.15 as measured by XPS. As long as copper remains on the surface, the substrate

is pinned to the metal monoxide concentration and cannot be fully reoxidized until the copper is eliminated. When the substrate is heated to $\geqslant 700$ K, copper is removed from the near-surface region by either desorption or diffusion back into the bulk, and the substrate is easily reoxidized to Co_3O_4 stoichiometry.

Phase equilibria studies by electromotive force (EMF) measurements have shown that the Co–Cu–O system forms thermodynamically stable $Cu_{1-x}Co_xO$ rocksalt solid solutions over the range of 1200–1350 K.[46] While the range of temperature is somewhat more harsh than the anneal temperature of 630 K used here, the electrochemical studies imply the formation of a mixed-metal rocksalt oxide to be plausible on the $Co_3O_4(110)$ substrate, particularly when the low partial pressure of oxygen (1.3×10^{-5} Pa) is taken into account. Whether the pinned monoxide surface has formed a completely homogeneous solid solution or whether phase separation to CuO, CoO, and/or $Cu_{1-x}Co_xO$ occurs cannot be fully ascertained. Mixed metal monoxides $M_xM'_{1-x}O$ (M and M', are $3d$ transition metals) can be synthesized as bulk powders by annealing MO/M′O mixtures under controlled oxygen environments at temperatures as low as 700 K. Since the solution forms through simple cation–cation interdiffusion, presumably the process could proceed at even lower temperatures if allowed to occur for a sufficiently long time.

Another Cu–Co–O solid solution, $Cu_xCo_{3-x}O_4$, is also known[47,48] and has been found to be stable in the bulk and relevant to heterogeneous processes that involve redox behavior.[9] The material's resistance to poisoning by SO_2 and its anticorrosion properties have been previously noted. The mixed-metal oxide is a partially inverted spinel with Cu^{2+} approximately divided in half between octahedral and tetrahedral sites, and cobalt filling the remaining cation spinel sites as Co^{3+}/Co^{2+}, as charge neutrality demands.[49] The material does not form over all potential values of x but tends to phase separate into CuO and $Cu_xCo_{3-x}O_4$ for $x>0.9$.

Both oxygen to cobalt concentrations (O/Co$\sim$1) and the Co $2p$ satellite structure rule out the formation of $Cu_xCo_{3-x}O_4$ as a dominant form of cobalt oxide on the copper segregated $Co_3O_4(110)$ surface. However, the present results have a potential impact on the nature of the $Cu_xCo_{3-x}O_4$ surface and its performance in corrosive environments, particularly those that depend upon a Co^{3+}/Co^{2+} redox couple for effective performance. If the surface of the $Cu_xCo_{3-x}O_4$ material becomes too high in copper content, our results suggest that an application might suffer from the inability to maintain Co^{3+} and/or an adequate surface oxygen concentration. Some phase separation occurs, as is evidenced by LEED. At a saturation Cu/Co concentration of 0.7, the copper content of the Cu-segregated surface is sufficiently high to induce phase separation in the $Cu_xCo_{3-x}O_4$ spinel.

V. CONCLUSIONS

The $Co_3O_4(110)$ single crystal surface has been successfully characterized using LEED, XPS, and AES. The AES and XPS spectra are consistent with a stoichiometric Co_3O_4 spinel surface. The cobalt $2p$ XP spectra have characteristic broadened, very weak satellites located at higher binding energies to the main peaks. LEED analysis of $Co_3O_4(110)$ showed a well-ordered pattern with sharp diffraction features. Upon annealing, Ca, K, Na, and Cu impurities segregated to the surface. The presence of copper was shown to correlate with reduction of the spinel surface to a CoO-like environment. The $Co_3O_4(110)$ substrate could not be fully reoxidized until all detectable copper had been removed from the surface.

ACKNOWLEDGMENTS

The authors gratefully acknowledge support from NSF under Grant No. CHE-0213320 and for the University of Nebraska Center for Materials Research and Analysis.

[1]Y. Iwasawa, Adv. Catal. **35**, 8822 (1987).
[2]J. Jansson, J. Catal. **194**, 55 (2000).
[3]B. A. Sexton, A. E. Hughes, and T. W. Turney, J. Catal. **97**, 390 (1986).
[4]V. E. Henrich and P. A. Cox, *The Surface Science of Metal Oxides* (Cambridge University Press, Cambridge, 1994).
[5]P. Thormahlen, M. Skoglundh, E. Fridell, and B. Anderson, J. Catal. **188**, 300 (1999).
[6]U.-S. Choi, G. Sakai, K. Shimanoe, and N. Yamazoe, Ceram. Eng. Sci. Proc. **24**, 101 (2003).
[7]O. R. Van Buskirk, E. I. Du Pont de Nemours and Co., U.S. Patent No. 4,310,596 (filed 1982).
[8]S. Angelov, D. Mechandjiev, B. Piperopv, V. Zarkov, A. Terlecki-Baricevic, D. Jovanovic, and Z. Jovanovic, Appl. Catal. **16**, 431 (1985).
[9]S. Angelov, G. Tyuliev, and T. Marinova, Appl. Surf. Sci. **27**, 381 (1987).
[10]J. L. Gautier, R. Rios, M. Garcia, J. F. Marco, and J. R. Gancedo, Thin Solid Films **311**, 51 (1997).
[11]J. G. Kim, D. L. Pugmire, D. Battaglia, and M. A. Langell, Appl. Surf. Sci. **165**, 70 (2000).
[12]*The Oxide Handbook*, edited by G. V. Samsonov (IFI/Plenum, New York, 1973).
[13]B. Marcus-Saubat, J. P. Beaufils, and Y. Barbaux, J. Chim. Phys. Phys.-Chim. Biol. **83**, 317 (1986).
[14]J. P. S. Badyal, X. Zhang, and R. M. Lambert, Surf. Sci. Lett. **255**, L15 (1990).
[15]Z. X. Shen *et al.*, Phys. Rev. B **42**, 1817 (1990).
[16]B. Pejova, A. Isahi, M. Najodski, and I. Grozdanov, MRS Bull. **36**, 161 (2001).
[17]G. A. Carson, M. H. Nassir, and M. A. Langell, J. Vac. Sci. Technol. A **14**, 1637 (1996).
[18]M. A. Langell, G. A. Carson, S. Smith, L. Peng, and M. H. Nassir, Mater. Res. Soc. Symp. Proc. **547**, 255 (1999).
[19]G. A. Carson, M. H. Nassir, and M. A. Langell, Surf. Sci. Spectra **5**, 235 (1998).
[20]T. J. Chuang, C. R. Brundle, and D. W. Rice, Surf. Sci. **59**, 413 (1976).
[21]V. M. Jimenez, A. Fernadez, J. P. Espinos, and A. R. Gonzales-Elipe, J. Electron Spectrosc. Relat. Phenom. **71**, 61 (1995).
[22]J. van Elp, J. L. Wieland, H. Eskes, P. Kuiper, G. A. Sawatasky, R. M. F. de Groot, and T. S. Turner, Phys. Rev. B **44**, 6090 (1991).
[23]M. Oku and Y. Sato, Appl. Surf. Sci. **55**, 37 (1992).
[24]M. A. Langell, C. W. Hutchings, G. A. Carson, and M. H. Nassir, J. Vac. Sci. Technol. A **14**, 1656 (1996).
[25]L. C. Davis, Phys. Rev. B **25**, 2912 (1982).
[26]N. S. McIntyre and M. G. Cook, Anal. Chem. **47**, 2208 (1975).
[27]L. J. Clarke, *Surface Crystallography: An Introduction to Low Energy Electron Diffraction* (Wiley, New York, 1985).
[28]Kindly provided through the generosity of W. H. McCarroll, Dept. Chemistry, Biochemistry, and Physics, Rider University, Lawrenceville, NJ.
[29]D. A. Shirley, Phys. Rev. B **5**, 4709 (1972).
[30]R. W. M. Kwok, available for downloading at http://www.phy.cuhk.edu.hk/~surface/xpspeak/

[31]M. A. Langell, J. G. Kim, D. L. Pugmire, and W. McCarroll, J. Vac. Sci. Technol. A **19**, 1977 (2001).
[32]D. Briggs and M. P. Seah, *Practical Surface Analysis* (Wiley, New York, 1990).
[33]N. S. McIntyre, D. D. Johnston, L. L. Coatsworth, R. D. Davidson, and J. R. Brown, Surf. Interface Anal. **15**, 265 (1990).
[34]M. A. Langell, G. A. Carson, M. Anderson, L. Peng, and S. Smith, Phys. Rev. B **59**, 4791 (1999).
[35]K. Wandelt, Surf. Sci. Rep. **2**, 1 (1982).
[36]B. W. Lee, J. A. Taylor, and J. W. Rabalais, Solid State Commun. **33**, 1205 (1980).
[37]M. Lenglet, R. Guillamet, J. Durr, D. Gryffroy, and R. E. Vandenberghe, Solid State Commun. **74**, 1035 (1990).
[38]L. E. Davis, N. C. MacDonald, P. W. Palmburg, G. E. Riach, and R. E. Weber, *Handbook of Auger Electron Spectroscopy* (Physical Electronics Industries, Perkin Elmer, Eden Prairie, MN, 1976).
[39]C. D. Wagner, W. M. Riggs, L. Davis, and J. F. Moulder, *Handbook of X-ray Photoelectron Spectroscopy* (Physical Electronics Industries, Perkin Elmer, Eden Prairie, MN, 1979).
[40]J. Haber, J. Stoch, and L. Ungier, J. Electron Spectrosc. Relat. Phenom. **9**, 459 (1976).
[41]J. Lahtinen, J. Vaari, A. Talo, A. Vehanen, and P. Hautojarvi, Vacuum **41**, 112 (1990).
[42]S. Angelov, E. Zhecheva, R. Stoyanova, and M. Atanasov, Phys. Chem. Solids **51**, 1157 (1990).
[43]Y. Oda, S. Mizuno, S. Todo, E. Torikai, and K. Hayakawa, Jpn. J. Appl. Phys., Part 1 **37**, 4518 (1998).
[44]M. W. Nydegger, G. Couderc, and M. A. Langell, Appl. Surf. Sci. **147**, 58 (1999).
[45]S. Chambers, *The Chemical Physics of Solid Surfaces*, edited D. P. Woodruff (Elsevier Science, Amsterdam, 2001), Vol. 9, p. 301.
[46]L. A. Zabdyr and O. B. Farichnaya, J. Phase Equilib. **23**, 149 (2002).
[47]K. Krezhov, K. Petrov, and T. Karamaneva, J. Solid State Chem. **48**, 33 (1983).
[48]I. Rasines, J. Appl. Crystallogr. **5**, 11 (1972).
[49]S. Angelov, E. Zhecheva, K. Petrov, and D. Mehandjiev, MRS Bull. **17**, 235 (1982).